AIP | Applied Physics Letters

Nanoscale measurements of local junction breakdown in epitaxial film silicon solar cells

M. J. Romero, K. Alberi, I. T. Martin, K. M. Jones, D. L. Young et al.

Citation: Appl. Phys. Lett. **97**, 092107 (2010); doi: 10.1063/1.3479534
View online: http://dx.doi.org/10.1063/1.3479534
View Table of Contents: http://apl.aip.org/resource/1/APPLAB/v97/i9
Published by the American Institute of Physics.

Nanoscale measurements of local junction breakdown in epitaxial film silicon solar cells

M. J. Romero,[a] K. Alberi, I. T. Martin, K. M. Jones, D. L. Young, Y. Yan, C. Teplin, M. M. Al-Jassim, P. Stradins, and H. M. Branz
National Renewable Energy Laboratory (NREL), 1617 Cole Boulevard Golden, Colorado 80401-3393, USA

(Received 14 June 2010; accepted 13 July 2010; published online 1 September 2010)

In this contribution, the authors report on near-field scanning optical microscopy measurements of the luminescence emitted from localized junction breakdown in epitaxial silicon solar cells. Our measurements suggest that the observed local reduction in breakdown voltage results from avalanche multiplication assisted by the reinforcing combination of (i) the local enhancement of the electrostatic field at the apex of inverted pyramid pits and (ii) the participation of defect states in the avalanche breakdown. Transmission electron microscopy reveals the microstructure of the defect responsible for the local junction breakdown. © *2010 American Institute of Physics*.
[doi:10.1063/1.3479534]

Silicon remains the leading semiconductor in terrestrial photovoltaics and will continue to dominate the production of solar cells for the foreseeable future. The expansion of the silicon production capacity is driving down the price of the feedstock but the costs associated to the fabrication of the wafers will continue at current levels. A *wafer replacement* approach, where crystalline silicon thin films are grown on inexpensive substrates, can provide high solar conversion efficiency and eliminate the expensive and energy-intensive wafer fabrication process.[1]

There are numerous strategies for achieving silicon epitaxy at the low temperatures compatible with inexpensive substrates.[2–9] Hot-wire chemical vapor deposition (HWCVD) is among the most attractive for solar cell manufacturing because it is easily scalable and capable of high epitaxial deposition rates.[10] In order to understand the basic aspects of the HWCVD silicon epitaxy[11] and the potential of epitaxial silicon solar cells, our early research efforts focus on the silicon homoepitaxy. Recently, we reported threading dislocation densities low enough ($\sim 10^5$ cm^{-2}) to meet the requirements for high efficiency. The density of dislocations correlates almost perfectly with the efficiency of the solar cell and, above $\sim 5\times 10^5$ cm^{-2}, is certainly the most significant contribution to recombination and efficiency loss.[12] At low dislocation densities below 10^5 cm^{-2}, on the other hand, we have to consider other factors limiting the efficiency. For example, we are dealing with high dark saturation currents ($J_0 \sim 10^{-7}$ A/cm^2) and the resulting degradation of the open-circuit voltage (best up-to-date V_{oc} is 568 mV).

In this letter, we investigate the processes responsible for the local junction breakdown observed in these cells because of their potential contribution to the degradation of the V_{oc}. Because of heat dissipation resulting from the high reverse current density at the breakdown sites, *thermography imaging* techniques are routinely used as diagnostics of electrical breakdown in silicon solar cells.[13,14] More recently, it has been shown that junction breakdown locations can be easily identified by *electroluminescence* (EL) *imaging* under reverse bias. This luminescence is primarily consistent with *bremsstrahlung* radiation[15,16] resulting from the acceleration of electrons and holes across the breakdown site and their subsequent deceleration. The emission spectrum (extending from the infrared into the visible spectrum) can be modeled as thermal radiation by simply assigning a chemical potential to the photons and introducing this chemical potential into Planck's radiation law. This is an interesting approach when correlating results from EL and *thermography imaging*. Here we introduce the application of near-field scanning optical microscopy (NSOM) in order to overcome the diffraction limit of conventional imaging methods and resolve at the nanoscale the processes involved in the local junction breakdown in epitaxial silicon solar cells.

As described in Ref. 12, heterojunction film silicon solar cells are fabricated on (100) n^+-type (As-doped, $\sim 10^{19}$ cm^{-2}) *Cz* silicon substrates, as shown in Fig. 1(a).

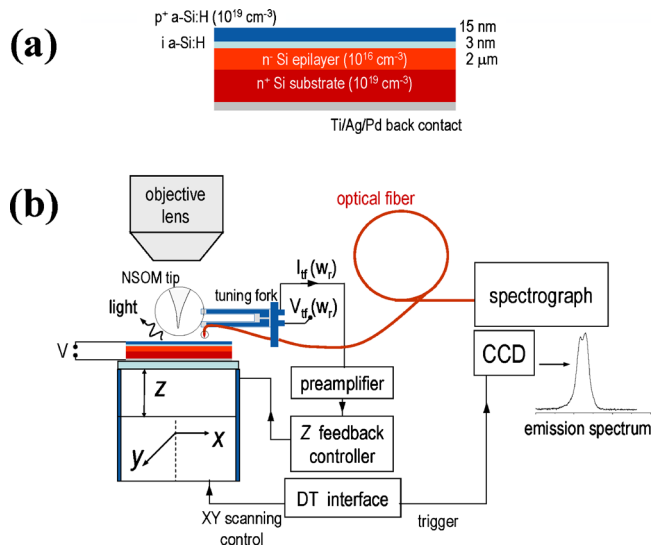

FIG. 1. (Color online) (a) Schematic of epitaxial silicon solar cell. (b) NSOM instrumentation for EL measurements. The sensor consists of a cantilevered and tapered optical fiber (collection mode) attached to a TF. The near-field luminescence detected by the optical fiber is directed to a spectrograph equipped with a CCD. EL imaging is accessible to the optical microscope integrated in this setup. The solar cells are reverse biased using a voltage source.

[a]Electronic mail: manuel.romero@nrel.gov. Tel.: (303)384-6653. FAX: (303)384-6604.

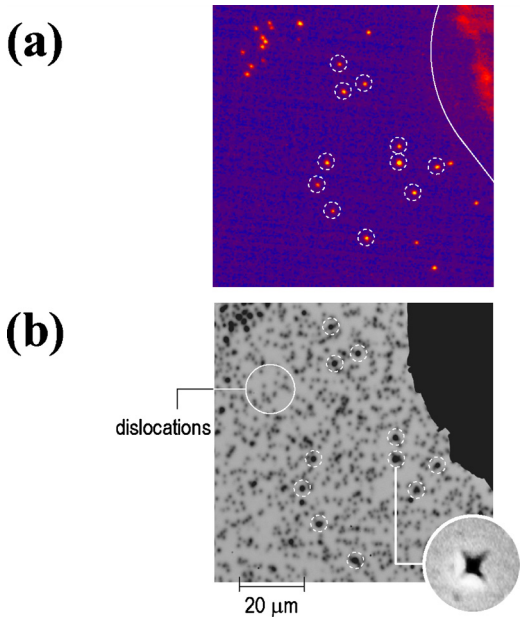

FIG. 2. (Color online) (a) Optical image of the *bremsstrahlung* radiation observed from the epitaxial silicon solar cells above the breakdown voltage of $V_r \sim 10$ V and (b) corresponding EBIC measurements performed in the FIB workstation. Every single location emitting this radiation corresponds to an inverted pyramid pit with a square base aligned with the ⟨100⟩ directions (inset). The electrical probe is seen at the top-right corner of the images.

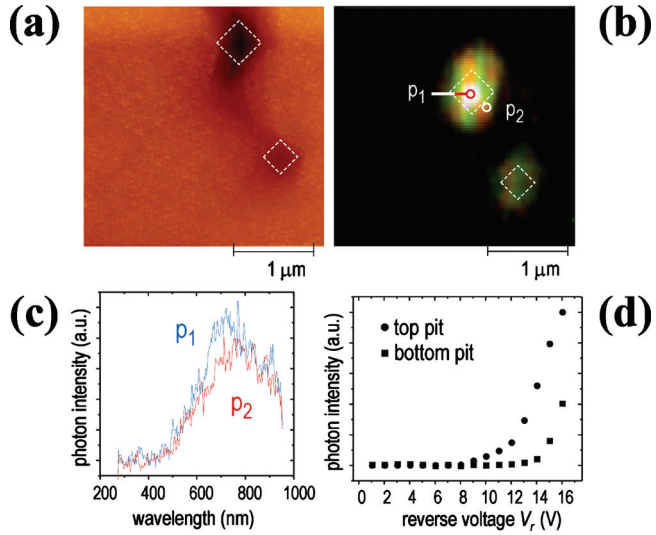

FIG. 3. (Color) *Microluminescence* from the pits. (a) Z-NSOM image and (b) corresponding photon intensity map of the EL (color coded to represent the local *shifting* in the emission spectrum). The *blueshift* in the *bremsstrahlung* radiation observed near the apex of the inverted pyramid [Fig. 3(c); spectrum at location p_1 on Fig. 3(b)] corresponds to the precise location where the breakdown initiates. (d) Bias dependence of the luminescence measured over the top and bottom inverted pyramid pits. The breakdown voltage is reduced for the well defined pit at the top of the Z-NSOM image. A 2×2 binning is applied to the NSOM photon intensity map in order to improve the signal-to-noise ratio. The spectrum data is not corrected.

After deposition of the *n*-type silicon epilayer by HWCVD (P-doped, $\sim 10^{16}$ cm^{-2}, thickness 2 μm), the solar cell is terminated with the deposition of an amorphous silicon emitter. Figure 1(b) shows the schematics of the NSOM setup. The sensor consists of a cantilevered and tapered optical fiber attached to a tuning fork (TF). The TF is driven by an oscillating voltage source near its resonance frequency $V_{tf}(\omega_r)$. The interaction between the tip and the specimen is monitored by the TF current $I_{tf}(\omega_r)$. We maintain a constant distance Z (in the near field) by controlling the amplitude of the TF oscillation during the scanning of the tip. One of the advantages of using a cantilevered optical fiber is that the tip can be viewed with the upright optical microscope and positioned accurately over the breakdown location. A voltage source provides the reverse bias to the solar cell (continuously or pulsed). The current is limited to I=25 mA to prevent permanent damage to the solar cells.

NSOM measurements are performed in the *spectrum imaging* mode. *Spectrum imaging* combines *spectroscopy* and *imaging* in one single measurement by acquiring the emission spectrum at high speed (typically 100 ms) in synchronization with the scanning of the NSOM tip. The digital electronics [DT interface in Fig. 1(b)] control the X-Y scanning of the tip and send the triggers to the charge-coupled device (CCD) electronics for the spectrum acquisition. After the scan is completed, the resulting *spectrum series* can be processed to reconstruct maps of the photon intensity (resolved in energy), photon energy, or to extract the spectrum for a selected area.

Figure 2(a) shows an optical image of the breakdown luminescence when applying a reverse bias $V_r \geq 10$ V. The precise locations where junction breakdown is initiated are easily discernible on the optical image. Further examination in a dual-beam focused-ion-beam (FIB) workstation, equipped with instrumentation for electron-beam-induced current (EBIC) measurements, reveals that every single location emitting this radiation corresponds to an inverted pyramid pit with a square base aligned in the ⟨100⟩ direction. These pits form spontaneously during the epitaxial growth and their dimension, aspect ratio, and density depend on the growth conditions and substrate surface preparation. The current loss at the pits is much greater than that seen at dislocations, so these defects are easily distinguished from one other in the EBIC image [see Fig. 2(b)]. The correspondence between Figs. 2(a) and 2(b) is evidence that locations undergoing electrical breakdown correspond to pits. Additional measurements show that the reverse is not true: not every single pit undergoes electrical breakdown.

To resolve the physics of the electrical breakdown at the nanoscale, we performed NSOM-based *spectrum imaging* measurements scanning one of the pits with an optical fiber tip, while applying a reverse bias to the cell. Figures 3(a) and 3(b) correspond to the NSOM image of the height and the measured photon intensity map of the EL for V_r=10 V and I=20 mA (color coded so that *red* and *blueshifts* in the emission spectrum are intuitive). For the well-defined pit at the top of Fig. 3(a) we observe a blueshift in the emission spectrum near the apex of the pyramid [Figs. 3(b) and 3(c)] which, in the *thermal radiation analogy*, corresponds to the location with the highest effective temperature of the electron distribution within the breakdown site (hence the blueshift). From the theory of *bremsstrahlung* radiation, the apex corresponds to the precise location where the breakdown initiates and the local field reaches its maximum [maximum acceleration of electrons (holes) across the site, hence the blueshift].[17] Fig. 3(d) shows the bias dependence of the luminescence measured over these pits. The abrupt increase in the photon intensity above the breakdown voltage is consistent with avalanche multiplication. The aspect ratio of the inverted pyramid is one of the most important factors deter-

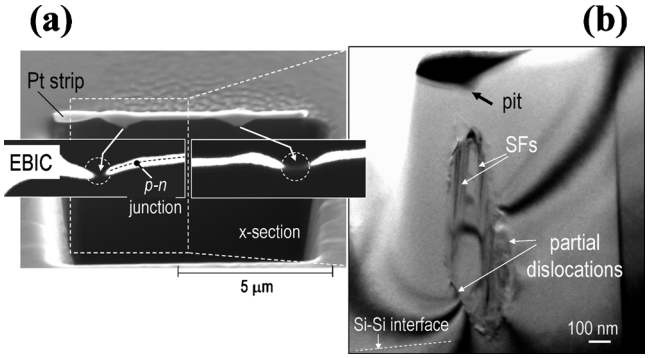

FIG. 4. (a) Secondary electron image of a FIB section and corresponding EBIC images from the pits. The collected current at the junction is significantly reduced near the apex of the pits. (b) TEM image of the structural defect associated with the local junction breakdown in these epitaxial silicon films. A strip of platinum is deposited *in situ* to preserve the surface during the ion milling.

mining the onset voltage for breakdown and the "likelihood" of the breakdown. For pits with higher aspect ratio, the more pronounced curvature at the apex results in a more intense local field (the *tip effect*) and, accordingly, a reduction in the breakdown voltage[18]—this is consistent with our observations; see Fig. 3(d).

To determine whether the avalanche multiplication is assisted by defect states or can be simply explained by geometrical effects (curvature of the apex), we investigated the evolution of the *p-n* junction by EBIC while sectioning through these pits in the FIB workstation. This provides a cross sectional view of the current reduction at the pits and complements the top EBIC image of Fig. 2(b). Figure 4(a) shows a secondary electron image of the FIB section and the measured EBIC signal. The degradation of the collected current near the apex of pits [circled regions in the EBIC insets of Fig. 4(a)] is consistent with a significant increase in Shockley–Read–Hall recombination within the depletion region. We have also observed that the higher the depletion-region recombination the lower the voltage onset for breakdown. All these findings strongly suggest that defect states participate in and facilitate the avalanche multiplication process.

We completed this investigation by preparing ultrathin sections for transmission electron microscopy (TEM). TEM observations reveal the existence of a structural defect associated with the local junction breakdown, as seen in the TEM image of Fig. 4(b). We find a complex structural defect in which two partial dislocations create a sequence of stacking faults (SFs) as they propagate in the film, finally annihilating (or recombining) near the surface in the vicinity of the pits' apex. A closer inspection at the substrate interface reveals that the partial dislocations originate in a region of lower density (possibly due to the presence of voids). Possible contamination at this interface is below our sensitivity limit. It is evident, however, that the formation of pits is associated with structural defects that nucleate at the interface and propagate in the epitaxial film. Presumably, further optimization of the epitaxial interface is necessary to eliminate both the structural defects and the pits.

In summary, we find that the dominant contribution to junction breakdown in these epitaxial silicon solar cells is avalanche multiplication localized at the apex of inverted pyramid pits. TEM analysis correlates the pits to defects in the underlying silicon film, which nucleate at the epitaxy interface. The avalanche multiplication process is assisted by the reinforcing combination of (i) the local enhancement of the electrostatic field at the apex of the inverted pyramid pit and (ii) the participation of defect states in the avalanche breakdown. The presence of a microstructural defect, in which two partial dislocations create a sequence of SFs as they propagate in the film, is further confirmation that the defect states participating in the avalanche multiplication can be related to this structural defect. The significant increase in recombination in the depletion region observed at these breakdown sites is a clear indication that eliminating these pits will be beneficial to V_{oc} and to the further development of epitaxial silicon solar cells.

This work was supported by the U.S. Department of Energy under Contract No. DE-AC36-08-GO28308.

[1]R. B. Bergmann, Appl. Phys. A: Mater. Sci. Process. **69**, 187 (1999).
[2]K. R. Catchpole, M. J. McCann, K. J. Weber, and A. W. Blakers, Sol. Energy Mater. Sol. Cells **68**, 173 (2001).
[3]A. G. Aberle, Thin Solid Films **511–512**, 26 (2006).
[4]H. Comfort, L. M. Garverick, and R. Reif, J. Appl. Phys. **62**, 3388 (1987); M. Kambara, H. Yagi, M. Sawayanagi, and T. Yoshida, *ibid.* **99**, 074901 (2006).
[5]Y. Mori, K. Yoshii, K. Yasutake, H. Kakiuchi, H. Ohmi, and K. Wada, Thin Solid Films **444**, 138 (2003).
[6]B. Rau, I. Sieber, B. Selle, S. Brehme, U. Knipper, S. Gall, and W. Fuhs, Thin Solid Films **451–452**, 644 (2004).
[7]A. G. Aberle, A. Straub, P. I. Widenborg, A. B. Sproul, Y. Huang, and P. Campbell, Prog. Photovoltaics **13**, 37 (2005).
[8]M. L. Terry, A. Straub, D. Inns, D. Song, and A. G. Aberle, Appl. Phys. Lett. **86**, 172108 (2005).
[9]P. I. Widenborg and A. G. Aberle, J. Cryst. Growth **306**, 177 (2007).
[10]I. T. Martin, C. W. Teplin, J. R. Doyle, H. M. Branz, and P. Stradins, J. Appl. Phys. **107**, 054906 (2010).
[11]C. W. Teplin, K. Alberi, M. Shub, C. Beall, I. Martin, M. J. Romero, D. L. Young, R. C. Reedy, P. Stradins, and H. M. Branz, Appl. Phys. Lett. **96**, 201901 (2010).
[12]K. Alberi, I. T. Martin, M. Shub, C. W. Teplin, M. J. Romero, R. C. Reedy, E. Iwaniczko, A. Duda, P. Stradins, H. M. Branz, and D. L. Young, Appl. Phys. Lett. **96**, 073502 (2010).
[13]M. Kasemann, W. Kwapil, M. C. Schubert, H. Habenicht, B. Walter, M. The, S. Kontermann, S. Rein, O. Breitenstein, J. Bauer, A. Lotnyk, B. Michl, H. Nagel, A. Schütt, J. Carstensen, H. Föll, T. Trupke, Y. Augarten, H. Kampwerth, R. A. Bardos, S. Pingel, J. Berghold, W. Warta, and S. W. Glunz, *Proceedings of the 33rd IEEE Photovoltaic Specialists Conference* (IEEE, San Diego CA, May 11–16, 2008), p. 148.
[14]W. Kwapil, M. Kasemann, P. Gundel, M. C. Schubert, W. Warta, O. Breitenstein, J. Bauer, A. Lotnyk, J.-M. Wagner, G. Coletti, and P. C. P. Bronsveld, *Proceedings of the 24th European Photovoltaic Solar Energy Conference and Exhibition* (WIP, Hamburg, Germany, September 21–25, 2009), p. 896.
[15]A. L. Lacaita, F. Zappa, S. Bigliardi, and M. Manfredi, IEEE Trans. Electron Devices **40**, 577 (1993).
[16]N. Akil, S. E. Kerns, D. V. Kerns, Jr., A. Hoffmann, and J.-P. Charles, Appl. Phys. Lett. **73**, 871 (1998).
[17]We observe a blueshift in the emission spectrum of the overall radiation emitted by the junction breakdown site when increasing the applied reverse bias.
[18]S. M. Sze and G. Gibbons, Solid-State Electron. **9**, 831 (1966).